Influence of South China Sea SST and the ENSO on Winter Rainfall over South China

ZHOU Lian-Tong (周连童)[*1,2], Chi-Yung TAM[2,3], Wen ZHOU(周文)[2,3], and Johnny C. L. CHAN[2,3]

[1]*Center for Monsoon System Research, Institute of Atmospheric Physics, Chinese Academy of Sciences, Beijing,100190*
[2]*CityU-IAP Laboratory for Atmospheric Sciences, City University of Hong Kong, Hong Kong*
[3]*Guy Carpenter Asia-Pacific Climate Impact Centre,School of Energy and Environment, City University of Hong Kong, Hong Kong*

(Submitted 30 May 2009; revised 10 August 2009)

ABSTRACT

The present study investigates the influence of South China Sea (SCS) SST and ENSO on winter (January–February–March; JFM) rainfall over South China and its dynamic processes by using station observations for the period 1951–2003, Met Office Hadley Center SST data for the period 1900–2008, and ERA-40 reanalysis data for the period 1958–2002. It is found that JFM rainfall over South China has a significant correlation with Niño-3 and SCS SST. Analyses show that in El Niño or positive SCS SST anomaly years, southwesterly anomalies at 700 hPa dominate over the South China Sea, which in turn transports more moisture into South China and favors increased rainfall. A partial regression analysis indicates that the independent ENSO influence on winter rainfall occurs mainly over southern areas of China, whereas SCS SST has a larger independent influence on winter rainfall in eastern China. The temperature over South China shows an obvious decrease at 300 hPa and an increase near the surface, with the former induced by Niño-3 and the latter SCS SST anomalies. This enhances the convective instability and weakens the potential vorticity (PV), which explains the strengthening of ascending motion and the increase of JFM rainfall over South China.

[*]Corresponding author: ZHOU Lian-Tong, zlt@mail.iap.ac.cn

Key words: ENSO, South China Sea, SST, rainfall, convective instability, potential vorticity

Citation: Zhou, L.-T., C.-Y. Tam, W. Zhou, and J. C. L. Chan, 2009: Influence of South China Sea SST and the ENSO on winter rainfall over South China. *Adv. Atmos. Sci.*, doi: 10.1007/s00376–009-9102-7.

1. Introduction

The ENSO cycle is an important subsystem of the global climate system. The ENSO often peaks in boreal winter, persists into spring and decays the following summer. Many studies have shown that the ENSO has a large impact on climate anomalies in East Asia (e.g. Fu and Teng, 1988; Huang and Wu, 1989; Huang et al.,1999; Wang et al., 2000; Wu et al., 2003; Zhou and Huang, 2003).

The interannual variations of the East Asian summer monsoon are closely associated with SSTs in the tropical Pacific (e.g. Chen, 1977; Huang and Wu, 1989; Nitta and Hu, 1996; Yang and Lau, 1998; Chang et al., 2000; Lau and Weng, 2001; Huang and Zhou, 2002; Huang et al., 2003; Wu et al., 2003; Yang and Lau, 2004; Lin and Lu, 2009). The relationship between SST and rainfall variability over South China has been studied (Chang et al., 2000; Wu et al., 2003; Chan et al., 2004; Chan and Zhou, 2005). The majority of previous studies on the effects of the ENSO on East Asian summer rainfall were carried out in the spring and summer. However, the influence of the ENSO on East Asian rainfall is not limited to summer (Zhang et al., 1999; Wang et al., 2000; Zhou and Wu, 2009). Zhang and Sumi (2002) showed there were positive precipitation anomalies

in winter (December–January–February; DJF) over southern areas of China during the El Niño mature phase. Wu et al. (2003) documented systematically ENSO effects on rainfall anomalies in other seasons, and showed a positive correlation between the ENSO and DJF rainfall over South China. Zhou and Wu (2009) also pointed out a significant positive correlation between the ENSO and winter (November–March) rainfall in the southeast of China.

The correlation between the ENSO and rainfall from December to May has been examined in this study (figure not shown). This study finds that there is a significant positive correlation between the Niño-3 SST and South China rainfall in January, February and March (JFM), but not in the traditional DJF winter months. Moreover, there is no significant correlation found for the other months covered by the study. The rainfall period considered in the present study differs slightly from previous studies (Zhang and Sumi, 2002; Wu et al., 2003), which have traditionally used the DJF mean. JFM rainfall over South China accounts for >20% of annual total rainfall (Fig. 1b), and, in addition, South China Sea (SCS) SST anomalies may also influence rainfall over South China. In the present study, therefore, we examine the influence of not only the ENSO, but also SCS SST on JFM rainfall over South China. In particular, we investigate the respective influences of the ENSO and SCS SST using partial regression and correlation analysis. The aim of this study is thus to investigate the influence of Niño-3 SST and SCS SST on JFM rainfall over South China.

The organization of the paper is as follows. Section 2 describes the datasets used in

the study. In Section 3, Influence of the ENSO and SCS SST on JFM rainfall over South China are analyzed. Section 4 presents circulation anomalies associated with the ENSO and SCS SST. Section 5 examines the influence of the ENSO and SCS SST on temperature anomalies. Section 6 examines the respective influence of the ENSO and SCS SST. Section 7 discusses the dynamical processes involved in the influence of thermal variability on rainfall over South China. And finally, a summary is provided in section 8.

2. Datasets

Monthly rainfall data from 160 stations in China (Fig. 1a) for the period 1951–2003, provided by the Chinese Meteorological Data Center, were used in the present study. These station observations were produced consistently throughout the observation period by the Chinese Meteorological Administration. For the purposes of this study, South China refers to the region from 110–125°E and 20–28°N, and the 28 stations in this South China region are also presented in Fig. 1a.

The study period covers several decades during which the NCEP–NCAR and ERA-40 reanalysis data provide possible options for study. Unfortunately, the NCEP-NCAR reanalysis dataset has been found to have large spurious changes during the study period (Yang et al., 2002; Inoue and Matsumoto, 2004; Wu et al., 2005). Thus, it was decided to use monthly mean wind, temperature, vertical velocity, humidity, and potential vorticity figures from the ERA-40 reanalysis dataset on a 2.5°×2.5° grid of the

European Centre for Medium-Range Weather Forecasts (ECMWF) (Gibson et al., 1997; Uppala, 2002), covering the period 1958–2002.

The monthly mean SST data on a 1°×1° grid were obtained from the Met Office Hadley Center, which covers the period 1900–2008 (Rayner et al., 2003).

3. Influence of the ENSO and SCS SST on JFM rainfall over South China

3.1 *Relationship between the ENSO, SCS SST and JFM rainfall*

The boreal winter (DJF) Niño-3 SST anomaly, averaged over the region of 5°S–5°N, 150°W–90°W, was taken as an index because winter is usually the mature phase of the ENSO (Rasmusson and Carpenter, 1982). The influence of the ENSO on rainfall over South China was analyzed through regression/correlation analyses between DJF Niño-3 and JFM rainfall in China. Figure 2a shows the regression of JFM rainfall with respect to DJF Niño-3 SST anomalies. As can be seen, there is a significant positive correlation (>0.05 level) region located over South China, indicating that JFM rainfall increases during El Niño years and decreases during La Niña years in this region. Such a relationship with the ENSO is consistent with previous studies (Zhang and Sumi, 2002; Wu et al., 2003).

To investigate regions where SST anomalies are related to South China rainfall variability, the regression of DJF SST with respect to JFM rainfall anomalies over South China was analyzed. JFM rainfall anomalies over South China are shown in Fig. 3a and Fig. 4 shows the regression of DJF SST with respect to JFM rainfall anomalies over

South China. From Fig. 4, a prominent feature is that there is significant positive correlation (>0.05 level) in the equatorial central and eastern Pacific. Thus, the mature phase of an El Niño event has a considerable influence on JFM rainfall in South China. Moreover, it is found that there is a significant positive correlation in the SCS region. This suggests that SCS SST anomalies may have an important influence on JFM rainfall over South China.

In order to investigate the above hypothesis, the relationship between SCS SST and JFM rainfall over South China was analyzed. The SCS SST anomaly averaged over the region of 10–20°N, 110–120°E is taken as a reference (Fig. 3b). Figure 2b shows the regression of JFM rainfall in China with respect to SCS SST anomalies. As can be seen, there is a significant positive correlation over South China, indicating that JFM rainfall increases during positive SCS SST anomaly years and decreases during negative SCS SST anomaly years. In comparison, the rainfall anomalies were smaller and extend more northward for SCS SST than for the ENSO.

In order to examine the relationship between SCS SST, the ENSO and winter rainfall, positive and negative rainfall anomaly cases were identified according to Fig. 3a and by the criterion that the area mean rainfall anomalies exceed $\pm$50 mm from the average. So, the selected positive rainfall anomaly cases are: 1959, 1969, 1975, 1983, 1985, 1990, 1992, 1997, and 1998 (a total of nine cases). Negative cases are: 1962, 1963, 1965, 1971, 1972, 1974, 1976, 1977, 1984, 1999, and 2002 (a total of eleven cases). The positive and negative SST anomalies corresponding to an increase or decrease in South China

rainfall are listed in Table 1. From Table 1, it can be seen that the best relationship exists for the years with an in-phase situation or SCS SST only. When an in-phase situation occurs, South China rainfall tends to bring positive anomalies (four out of nine cases) during the positive SST phase, however South China rainfall tends to bring negative anomalies (eight out of eleven cases) during the negative SST phase. On the contrary, in an out-of-phase situation, South China rainfall anomalies are more variable. During negative Niño-3 and the positive SCS SST phase, South China rainfall tends to bring more cases of positive anomalies (four out of nine cases), than negative anomalies (two out of eleven cases). However, South China rainfall can bring either positive (one out of nine cases) or negative anomalies (one out of eleven cases) during positive Niño-3 and negative SCS SST phases. Moreover, in the positive SCS SST phase only, South China rainfall tends to bring positive anomalies (eight out of nine cases), but in the negative SCS SST phase only it tends to bring negative anomalies (nine out of eleven cases). Thus, these results suggest that the Niño-3 and SCS SST anomalies have an important influence on rainfall over South China. Moreover, when SCS SST and Niño-3 SST are in phase, there is a reinforced influence on winter rainfall in the region. There are strong relationships between Niño-3 SST, SCS SST and South China rainfall above the 99% confidence level (see Table 2).

3.2 *Relationship between vertical velocity and water vapor flux and JFM rainfall*

In order to analyze the cause of rainfall anomalies over South China, regressions of

JFM vertical velocity (omega) and water vapor flux divergence with respect to the Niño-3 index and SCS SST anomalies, respectively, were utilized (Figs. 5a–d). A significant enhancement of ascent motion (Figs. 5a and 5b) and tropospheric moisture convergence (Figs. 5c and 5d) can be seen over South China corresponding to El Niño years and positive SCS SST anomalies, which is consistent with the rainfall increase. In comparison, rainfall, vertical motion, and moisture convergence anomalies extend somewhat more northward for the SCS SST than for the ENSO.

4. Influence of the ENSO and SCS SST on circulation over East Asia

Rainfall variability is closely related to atmospheric circulation changes. To understand the variability of JFM rainfall over South China, the effect of the ENSO and SCS on atmospheric circulation over East Asia is depicted by regression/correlation analysis between DJF Niño-3 and SCS SST and horizontal winds at 700 hPa and 200 hPa and a geopotential height of 500 hPa, respectively, over East Asia. Figures 6a and 6b show the regression of JFM horizontal winds at 700 hPa with respect to DJF Niño-3 and SCS SST anomalies, respectively, for the period of 1958–2002. From Fig. 6a, a prominent feature is anticyclonic circulation anomalies over the western North Pacific. To the northwest flank of this anomalous anticyclone are anomalous southwesterly winds along the southeast coast of China. These anomalous winds substantially enhance the moisture supply to southern areas of China, and these in turn contribute to increased JFM rainfall over South China. The present results are consistent with Wu et al. (2003), who

focused on winter (DJF) rainfall anomalies. The impact of the ENSO on East Asian rainfall through anomalous anticyclones has been extensively studied (Wang et al., 2000, Lau et al., 2004). However, the emphasis has been on summer. From Fig. 6b, the anticyclone also occurs over the western North Pacific, and anomalous southerlies also appear over South China. These features are similar to those in Fig. 6a, except that the anomalous anticyclone extends somewhat more northward for the SCS SST than for the ENSO. In comparison, the difference is that the significant northerly anomalies for the ENSO and westerly anomalies for SCS SST appeared over the mid latitudes in Asia. Along the southeast coast of China, the surface and 700-hPa winds are southwesterly in Fig. 6a, but southeasterly in Fig. 6b. Both types of winds contribute to above-normal rainfall in southern and eastern China.

Figures 6c and 6d show the regression of JFM geopotential height at 500 hPa with respect to DJF Niño-3 and SCS SST anomalies for the period 1958–2002. There are significant positive geopotential height anomalies over the western North Pacific. These indicate that anomalous anticyclones are intensified mainly over the SCS (Fig. 6c). From Fig. 6d, the anomalous geopotential height displaces northward, which corresponds to the northward displacement of anticyclones at 700 hPa.

At 200 hPa, there are anomalous cyclones to the north and south of the equatorial central Pacific and easterlies over the equator (Fig. 6e), as well as weak anomalous cyclones over the western North Pacific (Fig. 6f). Moreover, the anomalous cyclone extends somewhat more westward for the SCS SST than for the ENSO. There are

significant differences between SCS-SST-related and ENSO-related upper-level winds over northern areas of China.

The above wind anomalies are consistent with previous studies (e.g. Chang et al., 2000; Wang et al., 2000; Wu et al., 2003; Zhou and Wu, 2009). A key feature to note is the anomalous lower-level anticyclones over the western North Pacific and associated southwesterly winds to their northwest flanks. The southwesterly winds along the coast of China supply the moisture and contribute to the rainfall increase over southern and eastern China. The differences seen over the upper-level indicate that the SCS SST has a closer relationship with the circulation changes over mid latitudes in East Asia, as compared to those in the Niño-3 SST.

5. Influence of the ENSO and SCS SST on temperature over East Asia

Figure 7 shows JFM temperature anomalies at the surface, 700 hPa, and 300 hPa corresponding to a warm ENSO and SCS SST anomalies, respectively. The temperature anomalies display similar distributions for the SCS SST and the ENSO in the tropics. There are, however, pronounced differences in the magnitude and vertical structure in the subtropics and mid latitudes. At the surface and at 700 hPa, a positive SCS SST anomaly corresponds to large and positive temperature anomalies extending from western China to the western North Pacific (Figs. 7b and 7d), whereas a warm ENSO corresponds to small temperature anomalies, and in particular overland (Figs. 7a and 7c). The positive temperature anomalies over southeastern China are induced by positive ENSO or SCS

SST anomalies. This is confirmed by the regressed temperature advection at 700 hPa with respect to the SCS SST and Niño-3 SST anomalies, respectively, which are shown in Fig. 7. The positive temperature advection anomalies occur over South China and the SCS (Figs. 8a and 8b). This indicates that the positive temperature anomalies at the lower level may be induced by enhanced warm advection because of the ENSO or positive SCS SST. Moreover, the anomalous temperature advection extends somewhat more northward for the SCS SST than those for the ENSO. At 300 hPa, ENSO-related negative temperature anomalies extend from southern areas of China to the mid-latitude North Pacific (Fig. 7e). However, the SCS-related negative temperature anomalies appear over the North Pacific (Fig. 7f). In comparison, the magnitude is larger for the ENSO than for SCS SST. These negative temperature anomalies explain the upper-level cyclone wind anomalies over southern areas of China (Figs. 6e and 6f), which are expected from the thermal wind relationship.

Consistent with the differences seen in wind anomalies, the SCS-related and ENSO-related temperature anomalies have significant differences over the mid latitudes of Asia, and the anomalies over the tropics are similar.

6. Respective influence of the ENSO and SCS SST

Analyses in the previous section do not consider whether the ENSO and SCS SST are related or not. According to Table 2, the two are highly correlated, with a correlation coefficient of 0.40. This indicates that the anomalies as revealed by regression with

respect to Niño-3 SST or the SCS SST may not be independent.

In order to analyze the respective influences of SCS SST and the ENSO on rainfall, circulation and temperature anomalies, we a) removed SCS SST from the ENSO-related variability to obtain an ENSO-independent SCS SST ($T_{scs,\ res}$); and b) the ENSO from SCS-SST-related variability to obtain an SCS-SST-independent Niño3 SST ($T_{niño3,\ res}$). This was done by means of a linear regression as follows:

$$T_{scs,\ res} = T_{scs} - r_1(T_{scs}, T_{niño3}) \times T_{niño3},$$

$$T_{niño3,\ res} = T_{niño3} - r_2(T_{niño3}, T_{scs}) \times T_{scs},$$

where $r_{1(}r_{2)}$ is the regression coefficient of Niño3 SST ($T_{niño3}$)/SCS SST (T_{scs}) with respect to SCS SST (T_{scs}) /Niño3 ($T_{niño3}$).

After the ENSO signal and SCS SST were removed, respectively, regressions of rainfall, vertical velocity, and water vapor flux convergence at 700 hPa with respect to $T_{niño3,\ res}$ and $T_{scs,\ res}$ anomalies were produced, as shown in Fig. 9. In comparison, Niño3-SST-related rainfall anomalies are larger in southern areas of China, whereas SCS-SST-related rainfall anomalies are smaller, and the significant areas extend to higher latitudes (Figs. 9a and 9b). For both cases, the significant area and the magnitude of rainfall anomalies are smaller than those seen in Fig. 2. Differences consistent with those for rainfall anomalies are seen in vertical velocity and moisture convergence. For the ENSO, both the ascent and moisture convergence are over the southeast coast of China

(Figs. 9c and 9e). For SCS SST, the ascent and moisture convergence cover a less broad area in southern and eastern China and extend to higher latitudes (Figs. 9d and 9f). In comparison, the significant area and magnitude of vertical velocity and water flux convergence anomalies are smaller than those seen in Fig. 5. These results indicate that the independent ENSO influence on winter rainfall is mainly over South China and that SCS SST has a larger independent influence on winter rainfall in the northern part of South China.

The regressions of wind at 700 hPa, and temperature at 2 m and 300 hPa, with respect to $T_{niño3,\ res}$ and $T_{scs,\ res}$ anomalies, respectively, are shown in Fig. 10. After removing the SCS-SST-related part, the wind anomalies for the ENSO are similar to those seen in Figs. 6a (Fig.10a). However, the significant areas are less over southeastern areas of China. This indicates that SCS SST has a larger influence on mid-latitude Asian circulation changes. After removing the ENSO-related part, the wind anomalies for SCS SST are similar to those seen in Figs. 6b, except for the opposite wind anomalies in the tropics (Fig. 10b). This suggests that the tropical circulation anomalies are mostly due to the ENSO.

When the SCS-SST-related part is removed, the temperature anomalies at the surface associated with the ENSO become negative over southern areas of China, which is opposite to the situation depicted in Fig. 7a (Fig. 10c). At 300 hPa, negative temperature anomalies still appear over Southeast China, which are similar to those seen in Fig. 7e (Fig. 10e). After removing the ENSO-related part, the temperature anomalies in the

tropical Pacific and mid-latitude North Pacific associated with SCS SST are similar to those in Fig. 7b (Fig. 10d). However, at 300 hPa, the positive temperature anomalies are more significant and larger over southeast areas of China (Fig. 10f). The above results suggest that temperature changes associated with SCS SST and the ENSO are very different over East Asia. The ENSO makes a dominant contribution to temperature anomalies at the upper level, while SCS SST makes a dominant contribution to temperature anomalies at the surface over land in East Asia.

7. The dynamical process of the influence of thermal variability on rainfall

The results in previous sections show that the variability of JFM rainfall over South China is associated with circulation and temperature anomalies. However, the dynamical process for changes in JFM rainfall over South China is not clear. The decreases in upper-level temperature over South China are induced by the ENSO, while the increases in surface temperature are induced by SCS SST. This thermal variability may result in dynamical variability. Therefore, potential vorticity was analyzed because it is a synthetically physical term of dynamic and thermal state. The same method was used by Zhou and Huang (2009). Ertel (1942) pointed out that three-dimensional air-mass motion has a conservative property when the motion is adiabatic and non-frictional. Hoskins et al. (1985) made systematic investigations on the application of Ertel potential vorticity to atmospheric motion diagnosis. The vertical component of potential vorticity is as follows:

$$\mathrm{PV} = g(\xi + f)(-\frac{\partial \theta_{se}}{\partial p}), \qquad (1)$$

where g=9.8 m s^{-2} is the acceleration of gravity, ζ is relative vorticity, f is the Coriolis parameter, and θ_{se} is equivalent potential temperature.

The development of systematic potential vorticity depends on atmospheric stratification stability, baroclinicity, and vertical shear of wind. Generally speaking, the barotropic component is one order of magnitude larger than the baroclinic component (Wu and Liu, 2000). Therefore, the variability of potential vorticity mainly depends on its barotropic component and convective instability ($-\frac{\partial \theta_{se}}{\partial p}$). Thus, the variability of JFM potential vorticity anomalies was calculated using Eq.(1).

Figure 11 shows the regression of potential vorticity and convective instability at 700 hPa with respect to DJF Niño-3 and SCS SST anomalies, respectively. From Fig. 11a, it can be seen that negative potential vorticity anomalies cover South China. Similar potential vorticity anomalies can be observed in Fig. 9b, and are more extensive. These negative potential vorticity anomalies are related to the convective instability associated with different temperature changes at upper and lower levels. There are negative convective instability anomalies over most parts of South China and the southeast coast of China (Fig. 11c). Similar features can also be observed in Fig. 11d. This indicates a strengthening of convective instability associated with SCS SST or the ENSO over South China, which favors the enhancement of ascending motion and an increase in rainfall in South China. Furthermore, according to Eq. (1), an increase in vorticity may be inferred.

This suggests the development of cyclonic circulation anomalies over South China, which are helpful for enhancing local ascending flow, and thus increasing rainfall over the region.

8. Summary

The present analysis has identified an obvious significant positive correlation between the ENSO and JFM rainfall over South China. Moreover, SCS SST anomalies have been shown to have a considerable influence on JFM rainfall in the region. In addition, in in-phase years of SCS SST and ENSO, there exists a reinforced influence on JFM rainfall over South China. The influence of the ENSO and SCS SST on JFM circulation, temperature and potential vorticity anomalies have been analyzed to understand the cause of the JFM rainfall anomalies over South China and their dynamic process.

The results show that the anomalous southwesterly winds occur along the southeast coast of China in El Niño years or during positive SCS SST anomalies. These anomalous winds substantially enhance the moisture supply to southern China and contribute to an increase in JFM rainfall in the region. The differences are that anomalous anticyclones extend somewhat more northward for SCS SST than for the ENSO. These partial regression results indicate that the independent ENSO influence on winter rainfall is mainly over South China and that SCS SST has a larger independent influence on winter rainfall in the northern part of South China. Moreover, the rainfall anomalies are smaller

for SCS SST than for the ENSO. The results also show that negative temperature anomalies occur over South China at upper levels and that positive temperature anomalies occurring at lower levels are induced by Niño-3 SST and SCS SST, respectively. These indicate that the ENSO has a dominant contribution to temperature anomalies at the upper level, while SCS SST has a dominant contribution to temperature anomalies at the surface overland in East Asia. The differing thermal variability enhances convective instability over South China and decreases potential vorticity, which may infer an increase in vorticity, which in turn contributes to a strengthening of ascending motion and the development of cyclonic circulation and an increase in JFM rainfall over South China.

Acknowledgments. The authors appreciate the comments of the two anonymous reviewers, which led to significant improvements in the manuscript. This research was supported by the National Basic Research Program of China (Grant No. 2009CB421405), the National Natural Science Foundation of China (Grant No. 40730952 and 40905027), the Program of Knowledge Innovation for the third period, the Chinese Academy of Sciences (Grant No. KZCX2-YW-220), and City University of Hong Kong Strategic Research Grants 7002231 and 7002329.

REFERENCES

Chan, J. C. L., Y. M. Liu, K. C. Chow, Y. H. Ding, W. K. M. Lau, and K. L. Chan, 2004: Design of a regional climate model for the simulation of South China summer monsoon rainfall. *J. Meteor. Soc. Japan*, **82**, 1645-1665.

Chan, J. C. L., and W. Zhou, 2005: PDO, ENSO and the early summer monsoon rainfall over south China. *Geophys. Res. Let.*, **32**, L08810, doi:10.1029/2004GL022015.

Chang, C. P., Y. Zhang, and T. Li, 2000: Interannual and interdecadal variations of the East Asian summer monsoon and tropical Pacific SSTs. Part II: Meridional structure of the monsoon. *J. Climate*, **13**, 4326-4340.

Chen, L. T., 1977: Impact of the SST anomalies in the equatorial eastern Pacific on the tropical atmospheric circulation and rainfall during the rainy period in China. *Chinese J. Amos. Sci*.,**1**, 1-12. (in Chinese)

Ertel, H., 1942: Ein neuer hydrodynamischer wirbelsatz. *Meteorolog*. Zeitschr Braun-schweig, **59**, 277-281.

Fu, C.B., and X. L. Teng, 1988: Climate anomalies in China associated with El Niño/Southern Oscillation. *Chinese J. Atmos. Sci*., Special Issue, 133-141. (in Chinese)

Gibson, J. K., P. Kallberg, S. Uppala, A. Hernandez, A. Normura, and E. Serrano, 1997: ERA description, ECMWF reanalysis project report series1, ECMWF. *Reading*, 66pp.

Hoskins, B. J., M. E. McIntyre, and A. W. Robertson, 1985: On the use and significance of isentropic potential vorticity maps. *Quart. J. Roy. Meteor. Soc*., **111**, 877-946.

Huang, R. H., and Y. F. Wu, 1989: The influence of ENSO on the summer climate change in China and its mechanisms. *Adv. Atmos. Sci.*, **6**, 21-32.

Huang, R. H., Y. H. Xu, and L. T. Zhou, 1999: The interdecadal variation of summer rainfall in China and the drought trend in North China. *Plateau Meteorology*, **18**, 465-475. (in Chinese)

Huang, R. H., and L. T. Zhou, 2002: Research on the characteristics, formation mechanism and prediction of severe climate disasters in China. *Journal of Natural Disasters*, **11**, 1-9. (in Chinese)

Huang, R.H., L.T. Zhou, and W. Chen, 2003: The progresses of recent studies on the variabilities of the East Asian monsoon and their causes. *Adv. Atmos. Sci.*, **20**, 55-69.

Inoue, T., and J. Matsumoto, 2004: A comparison of summer sea level pressure over East Eurasia between NCEP/NCAR reanalysis and ERA-40 for the period 1960-99. *J. Meteor. Soc. Japan*, **82**, 951-958.

Lau, K. M., and H. Y. Weng, 2001: Coherent model of global SST and summer rainfall over China: An assessment of the regional impacts of the 1997-98 El Niño. *J. Climate*, **14**, 1294-1208.

Lau, N. C., M. J. Nath, and H. Wang, 2004: Simulation by a GFDL GCM of ENSO-related variability of the coupled atmosphere-ocean system in the East Asian monsoon region. *East Asian Monsoon*, C.-P, Chang, Ed., World Scientific Publishing Co., 271-300.

Lin, Z. D., and R. Y. Lu, 2009: The ENSO's effect on Eastern China rainfall in the following early summer. *Adv. Atmos. Sci.*, **26**, 333-342, doi: 10.1007/s00376-009-0333-4.

Nitta, T., and Z. Z. Hu, 1996: Summer climate variability in China and its association with 500-hPa height and tropical convection. *J. Meteor. Soc. Japan*, **74**, 425-445.

Rasmusson, E. M., and T. H. Carpenter, 1982: Variations in tropical sea surface temperature and surface wind fields associated with the Southern Oscillation/El Niño. *Mon. Wea. Rev.*, **110**, 354-384.

Rayner, N. A., D. E. Parker, E. B. Horton, C. K. Folland, L. V. Alexander, D. P. Rowell, E. C. Kent, and A. Kaplan, 2003: Global analyses of sea surface temperature, sea ice,

and night marine air temperature since the late nineteenth century. *J. Geophys. Res.*, **108**(D14), 4407,doi:10.1029/2002JD002670.

Uppala, S., 2002: ECMWF reanalysis,1957-2001, ERA-40. *ERA-40 Project Report Series*, **3**, 1-10.

Wang, B., R. Wu, and X. Fu, 2000: Pacific –East Asian teleconnection: How does ENSO affect East Asian climate? *J. Climate*, **13**, 1517-1536.

Wu, G. X., and Y. M. Liu, 2000: Thermal adaptation, overshooting, dispersion, and subtropical anticyclone. Part I: Thermal adaptation and overshooting. *Chinese J. Atmos. Sc.*, **24**, 433-446. (in Chinese)

Wu, R., Z. Z. Hu, and B. P. Kirtman, 2003: Evolution of ENSO-related rainfall anomalies in East Asia and the processes. *J. Climate*, **16**, 3741-3757.

Wu, R., III. J. L. Kinter, and B. P. Kirtman, 2005: Discrepancy of interdecadal changes in the Asian region among the NCEP-NCAR reanalysis, objective analyses, and observations. *J. Climate*, **18**, 3048-3067.

Yang, F. L., and K. M. Lau, 2004: Trend and variability of China precipitation in spring and summer: linkage to sea-surface temperatures. *International Journal of Climatology*, DOI:10.1002/joc.1094.

Yang, S., and K.M. Lau, 1998: Influences of sea surface temperature and ground wetness on Asian summer monsoon. *J. Climate*, **11**, 3230-3246.

Yang, S., K. M. Lau, and K. M. Kim, 2002: Variations of the East Asian jet stream and Asian-Pacific-American winter climate anomalies. *J. Climate*, **15**, 306-325.Zhang, R. H., A. Sumi, and M. Kimoto, 1999: A diagnostic study of the impact of El Niño on the precipitation in China. *Adv. Atmos. Sci.*, **16**, 229-241.

Zhang, R. H., and A. Sumi, 2002: Moisture circulation over East Asia during El Niño episode in Northern winter, spring and autumn. *J. Meteor. Soc. Japan*, **80**, 213-227.

Zhou, L. T., and R. H. Huang, 2003: Research on the characteristics of interdecadal

variability of summer climate in China and its possible cause. *Climatic and Environmental Research*, **8**, 274-290. (in Chinese)

Zhou, L. T., and R. H. Huang, 2009: Interdecadal variability of summer rainfall in Northwest China and its possible causes. *International Journal of Climatology*, DOI:10.1002/joc.1923.

Zhou, L. T., and R. Wu, 2009: Respective impacts of East Asian winter monsoon and ENSO on winter rainfall in China. *J. Geophys. Res.*,(accept).

Figure Captions:

Table 1. Positive and negative South China rainfall anomalies during different phases of El Niño.

Table 2. Correlation coefficients between the Niño-3 SST index, SCS SST and South China rainfall during the period 1958–2002.

Fig. 1. (a) The 160 stations used for rainfall data and their locations (a "1" indicates a station in South China); (b) percentage of annual total rainfall in JFM.

Fig. 2. Regression of rainfall (units: mm) with respect to normalized DJF Niño-3 SST (a) and SCS SST (b). Shading denotes regions with correlation significant at 0.05 level.

Fig. 3. Time series of JFM rainfall anomalies over South China (a) (units: mm), DJF Niño-3 SST (solid curves), and DJF SCS SST (dashed curve) (b) (units: ℃).

Fig. 4. Regression of DJF SST with respect to normalized JFM rainfall anomalies over South China for the period 1958–2002 (units: ℃). Shading denotes regions with correlation significant at 0.05 level.

Fig. 5. Regression of 700-hPa vertical velocity (units: Pa s^{-1}) (a) and water vapor flux convergence (integration 1000–100 hPa) (units: g m^{-2} s^{-1}) (c) with respect to normalized DJF Niño-3 SST. (b) and (d) are the same as (a) and (c) except for SCS SST. Shading denotes regions with correlation significant at 0.05 level.

Fig. 6. Regression of JFM 700-hPa wind (units: m s^{-1}) (a), 500-hPa geopotential height (units: gpm) (c) and 200-hPa wind (units: m s^{-1}) (e) with respect to normalized DJF Niño-3 SST. (b), (d), and (f) are the same as (a), (c), and (e) except for SCS SST. Shading denotes regions with correlation significant at 0.05 level. The significance in (a) and (b) is based on the correlation with *v*-wind and that in (e) and (f) is based on the correlation with *u*-wind.

Fig. 7. Regression of JFM surface temperature at 2 m (a), 700-hPa (c), and 300-hPa (e) (units: ℃) with respect to normalized DJF Niño-3 SST. (b), (d), and (f) are the same as (a), (c), and (e) except for SCS SST. Shading denotes regions with correlation significant at 0.05 level.

Fig. 8. Regression of JFM 700-hPa temperature advection (units: 10^5 ℃ s^{-1}) with respect to normalized DJF Niño-3 SST (a) and SCS SST (b). Shading denotes regions with correlation significant at 0.05 level.

Fig. 9. Regression of rainfall (units: mm) (a), 700-hPa vertical velocity (units: Pa s^{-1}) (c) and water vapor flux convergence (integration 1000–100 hPa) (units: g m^{-2} s^{-1}) (e) with respect to normalized DJF $T_{niño3,\ res}$. (b), (d), and (f) are the same as (a), (c), and (e) except for $T_{scs,\ res}$. Shading denotes regions with correlation significant at 0.05 level.

Fig. 10. Regression of JFM 700-hPa wind (units: m s^{-1}) (a), surface (2 m) (c), and 300 hPa (e) temperature (units: ℃) with respect to normalized DJF $T_{niño3,\ res}$. (b), (d), and (f) are the same as (a), (c), and (e) except for DJF $T_{scs,\ res}$. Shading denotes regions with correlation significant at 0.05 level. The significance in (a) and (b) is based on the correlation with *v*-wind.

Fig. 11. Regression of JFM 700-hPa potential vorticity (units: 10^6 K m^2 Kg^{-1} s^{-1}) (a) and convective instability (c) (units: 10^5 K Pa^{-1}) with respect to normalized DJF Niño-3 SST. (b) and (d) are the same as (a) and (c) except for DJF SCS SST. Shading denotes regions with correlation significant at 0.05 level.

Table 1. Positive and negative South China rainfall anomalies during different phases of El Niño.

	Positive South China rainfall	Negative South China rainfall
Positive Niño-3 and SCS SST	1969, 1983, 1992, 1998	
Positive Niño-3 and negative SCS SST	1959,	1977
Negative Niño-3 and positive SCS SST	1975, 1985, 1990, 1997	1999, 2002
Negative Niño-3 and SCS SST		1962, 1963, 1965, 1971, 1972, 1974, 1976, 1984

Table 2. Correlation coefficients between the Niño-3 SST index, SCS SST and South China rainfall during the period 1958–2002.

	South China rainfall	SCS SST
Niño-3 SST	0.54**	0.40**
SCS SST	0.39**	

**:significant > 0.01 level.

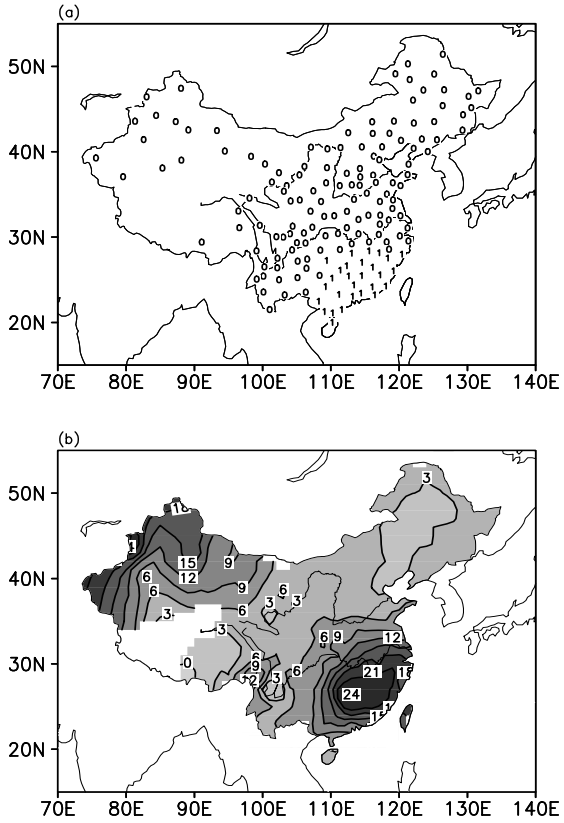

Fig. 1. (a) The 160 stations used for rainfall data and their locations (a "1" indicates a station in South China); (b) percentage of annual total rainfall in JFM.

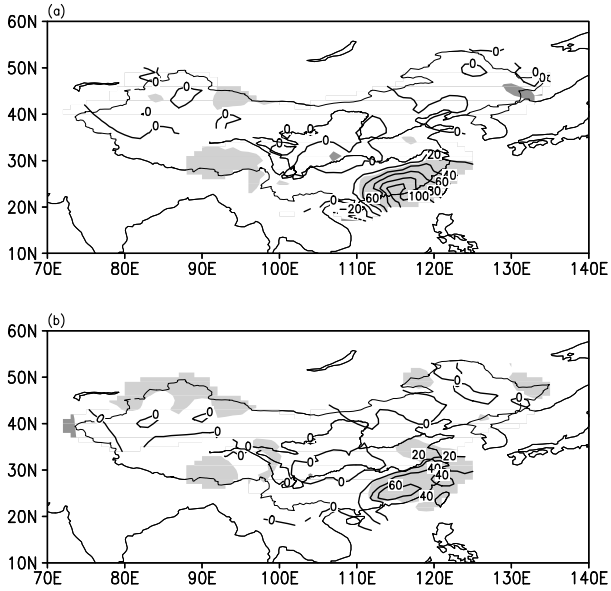

Fig. 2. Regression of rainfall (units: mm) with respect to normalized DJF Niño-3 SST (a)

and SCS SST (b). Shading denotes regions with correlation significant at 0.05 level.

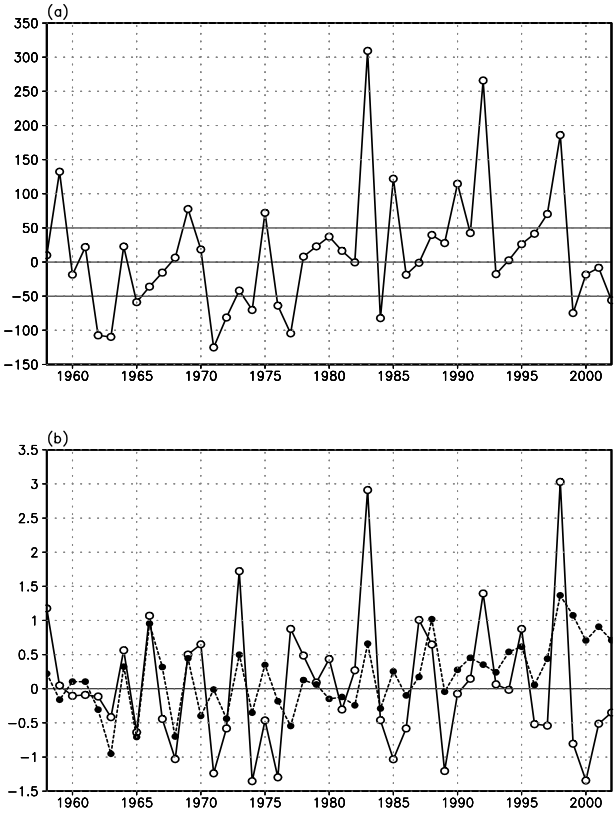

Fig. 3. Time series of JFM rainfall anomalies over South China (a) (units: mm), DJF Niño-3 SST (solid curves), and DJF SCS SST (dashed curve) (b) (units: ℃).

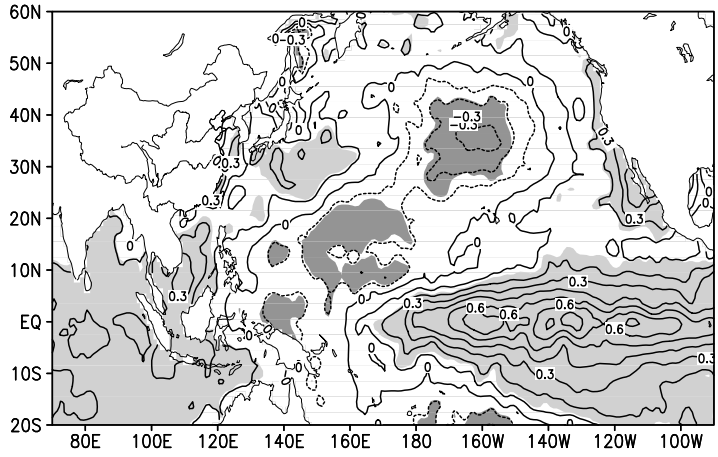

Fig. 4. Regression of DJF SST with respect to normalized JFM rainfall anomalies over South China for the period 1958–2002 (units: ℃). Shading denotes regions with correlation significant at 0.05 level.

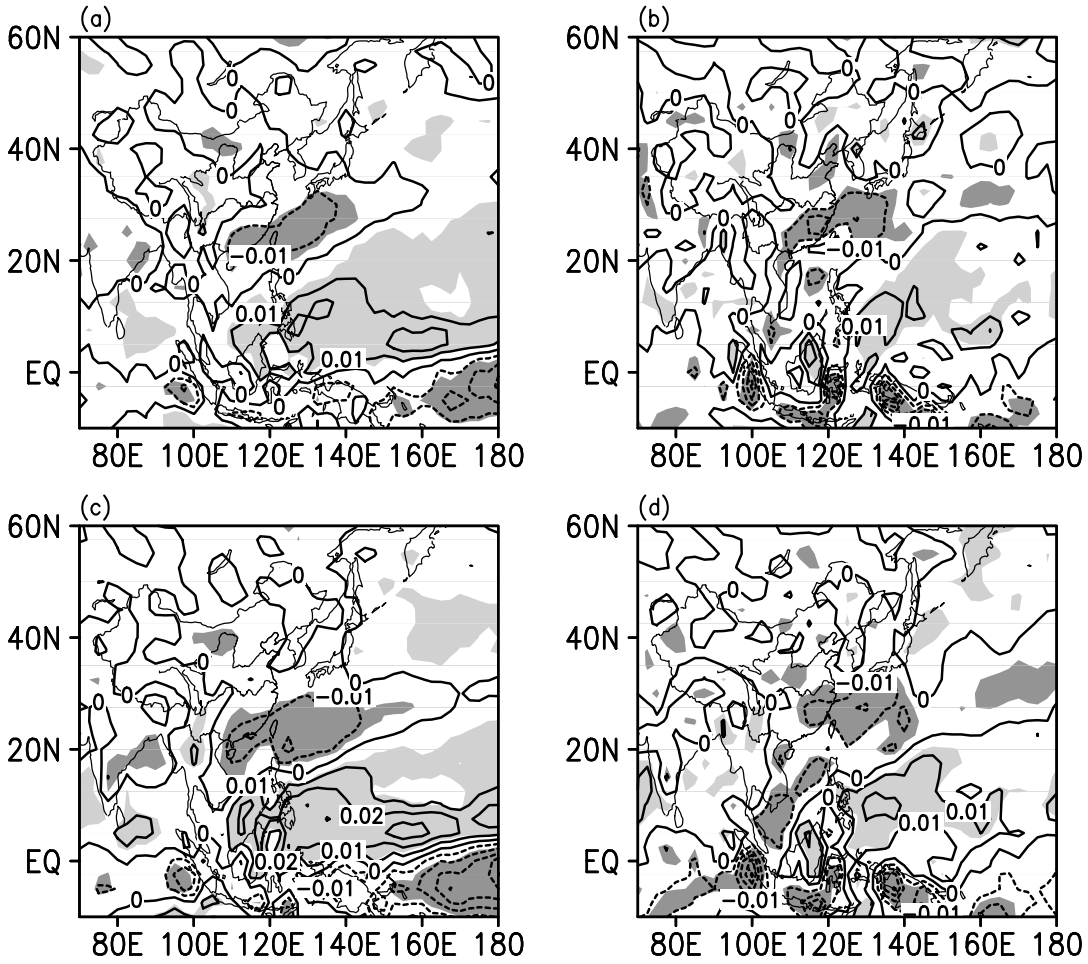

Fig. 5. Regression of 700-hPa vertical velocity (units: Pa s^{-1}) (a) and water vapor flux convergence (integration 1000–100 hPa) (units: g m^{-2} s^{-1}) (c) with respect to normalized DJF Niño-3 SST. (b) and (d) are the same as (a) and (c) except for SCS SST. Shading denotes regions with correlation significant at 0.05 level.

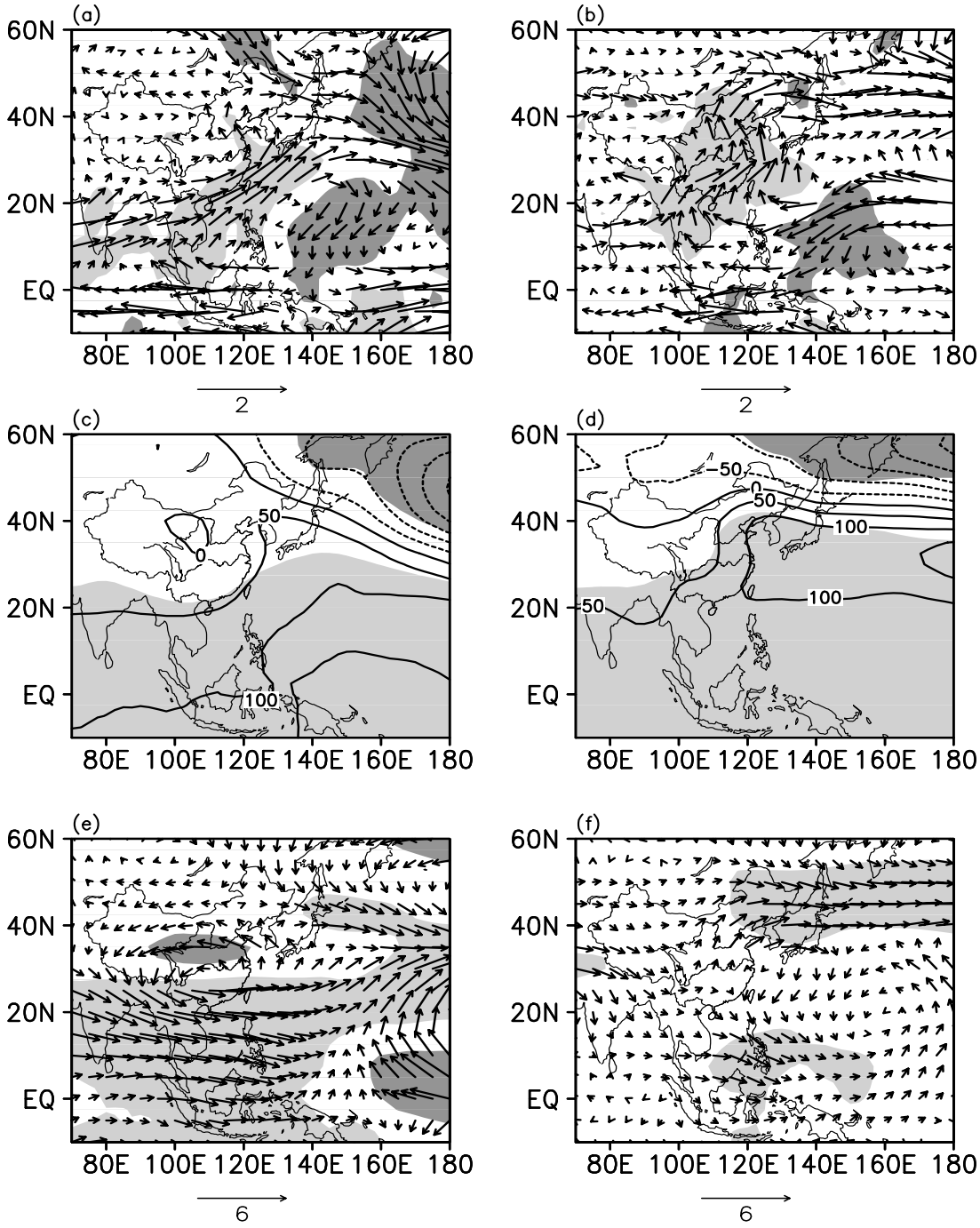

Fig. 6. Regression of JFM 700-hPa wind (units: m s^{-1}) (a), 500-hPa geopotential height (units: gpm) (c) and 200-hPa wind (units: m s^{-1}) (e) with respect to normalized DJF Niño-3 SST. (b), (d), and (f) are the same as (a), (c), and (e) except for SCS SST. Shading denotes regions with correlation significant at 0.05 level. The significance in (a) and (b)

is based on the correlation with v-wind and that in (e) and (f) is based on the correlation with u-wind.

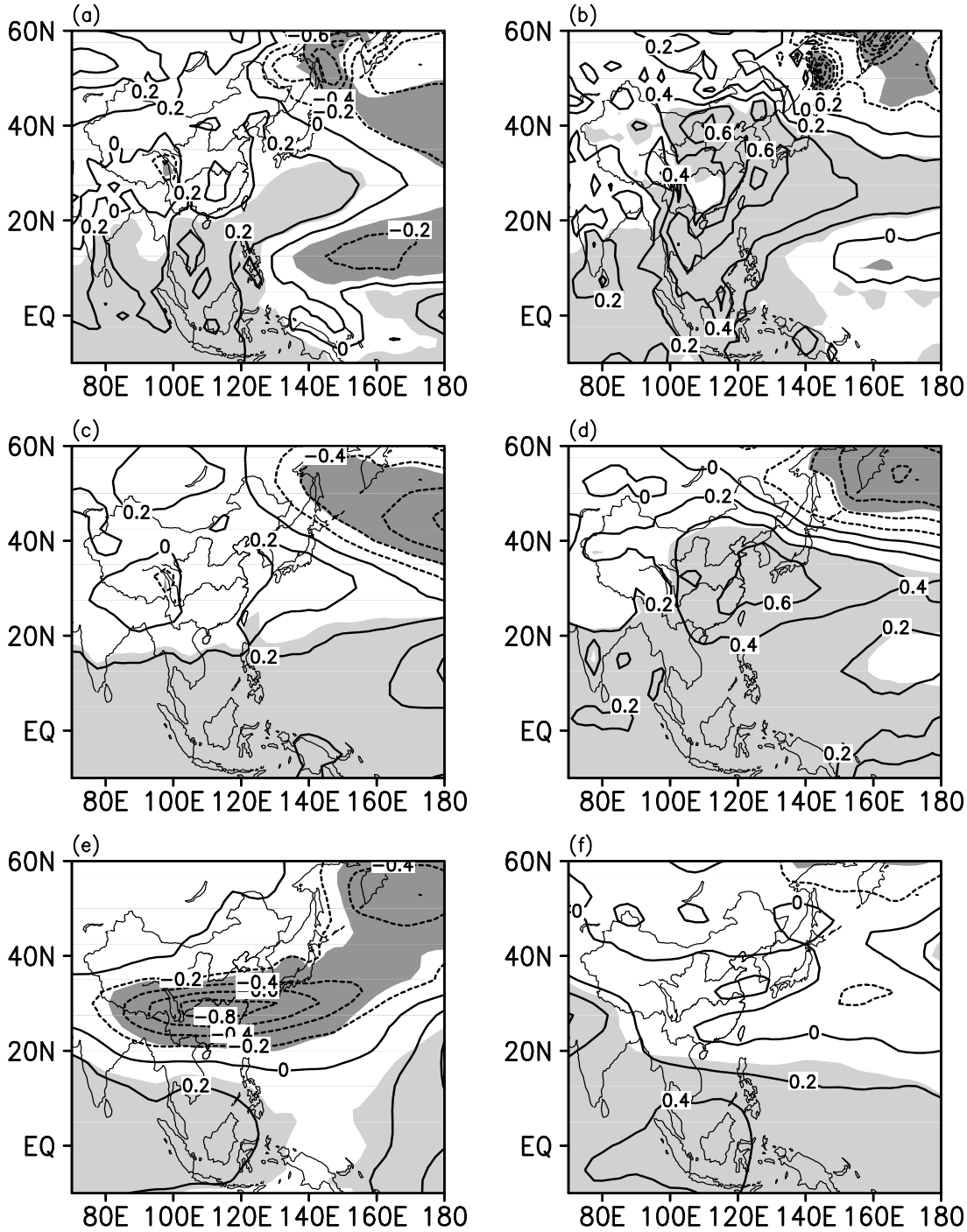

Fig. 7. Regression of JFM surface temperature at 2 m (a), 700-hPa (c), and 300-hPa (e)

(units: ℃) with respect to normalized DJF Niño-3 SST. (b), (d), and (f) are the same as (a), (c), and (e) except for SCS SST. Shading denotes regions with correlation significant at 0.05 level.

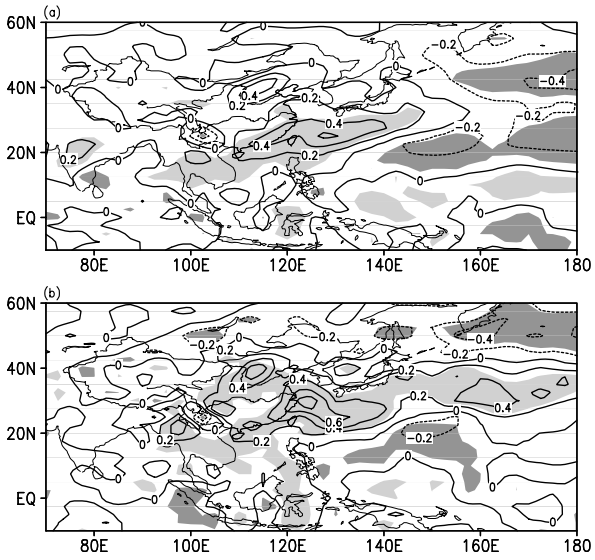

Fig. 8. Regression of JFM 700-hPa temperature advection (units: 10^5 ℃ s^{-1}) with respect to DJF Niño-3 SST (a) and SCS SST (b). Shading denotes regions with correlation significant at 0.05 level

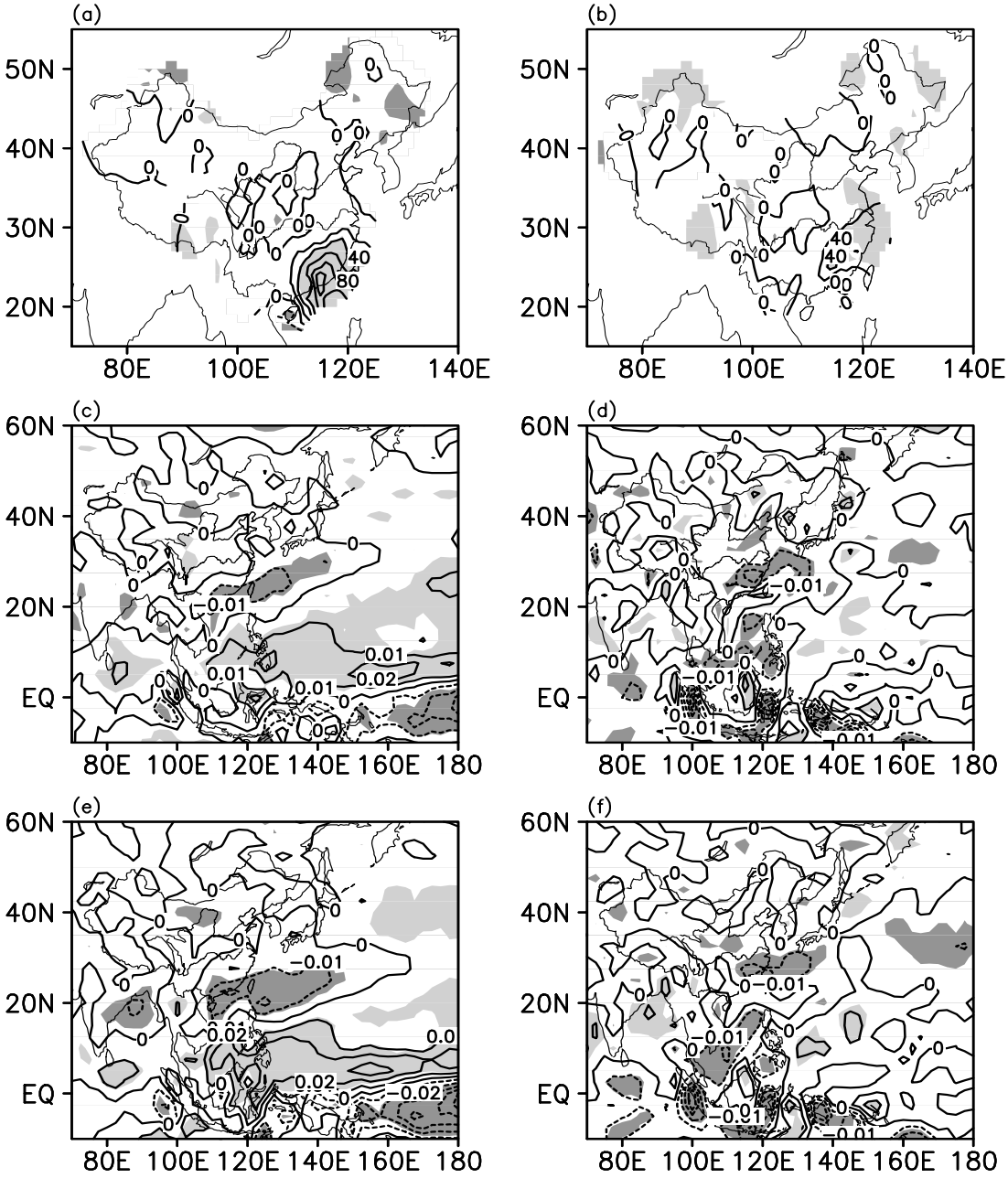

Fig. 9. Regression of rainfall (units: mm) (a), 700-hPa vertical velocity (units: Pa s^{-1}) (c) and water vapor flux convergence (integration 1000–100 hPa) (units: g m^{-2} s^{-1}) (e) with respect to normalized DJF $T_{niño3,\ res}$. (b), (d), and (f) are the same as (a), (c), and (e) except for $T_{scs,\ res}$. Shading denotes regions with correlation significant at 0.05 level.

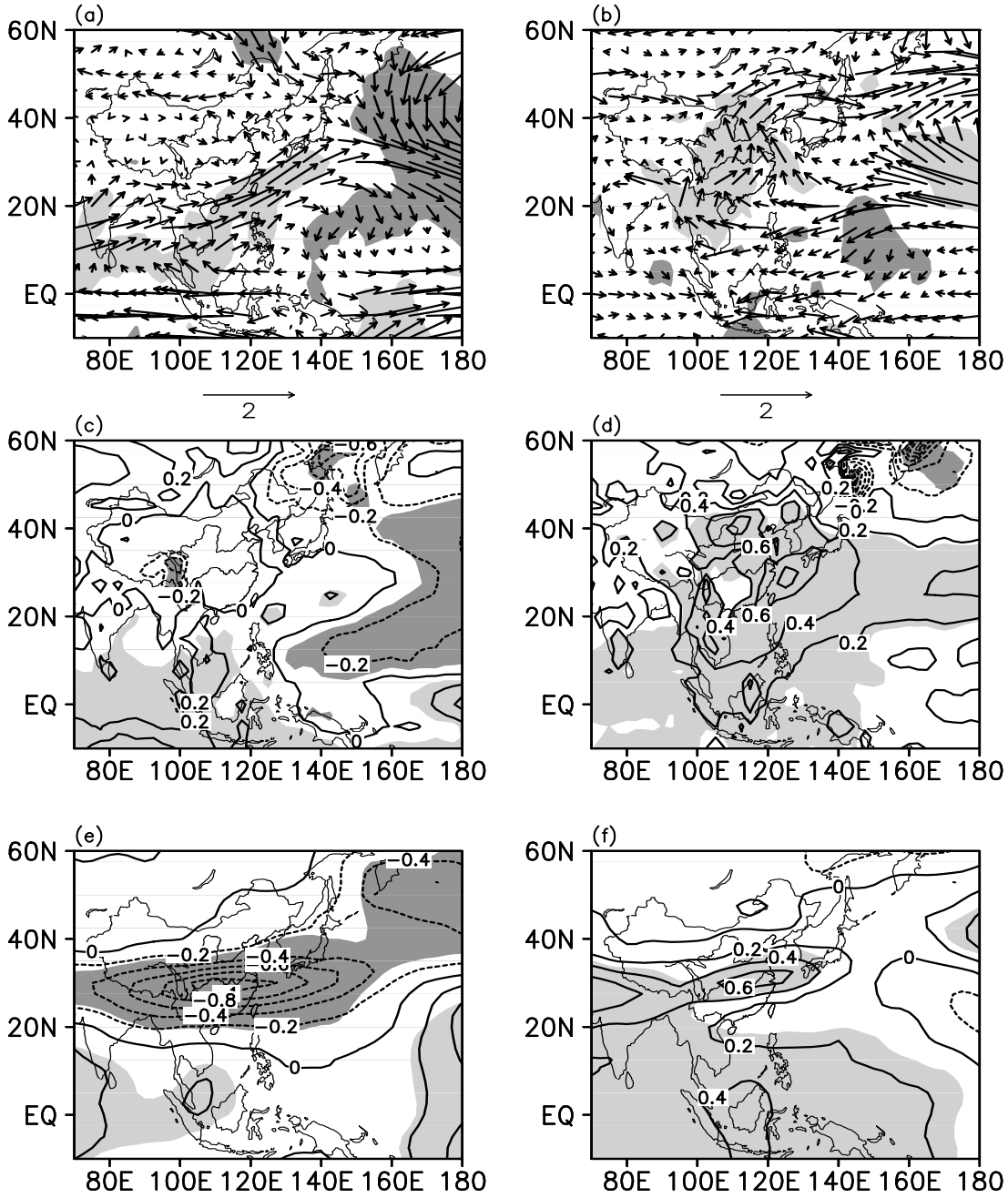

Fig. 10. Regression of JFM 700-hPa wind (units: m s^{-1}) (a), surface (2 m) (c), and 300 hPa (e) temperature (units: ℃) with respect to normalized DJF $T_{niño3,\ res}$. (b), (d), and (f) are the same as (a), (c), and (e) except for DJF $T_{scs,\ res}$. Shading denotes regions with correlation significant at 0.05 level. The significance in (a) and (b) is based on the correlation with v-wind.

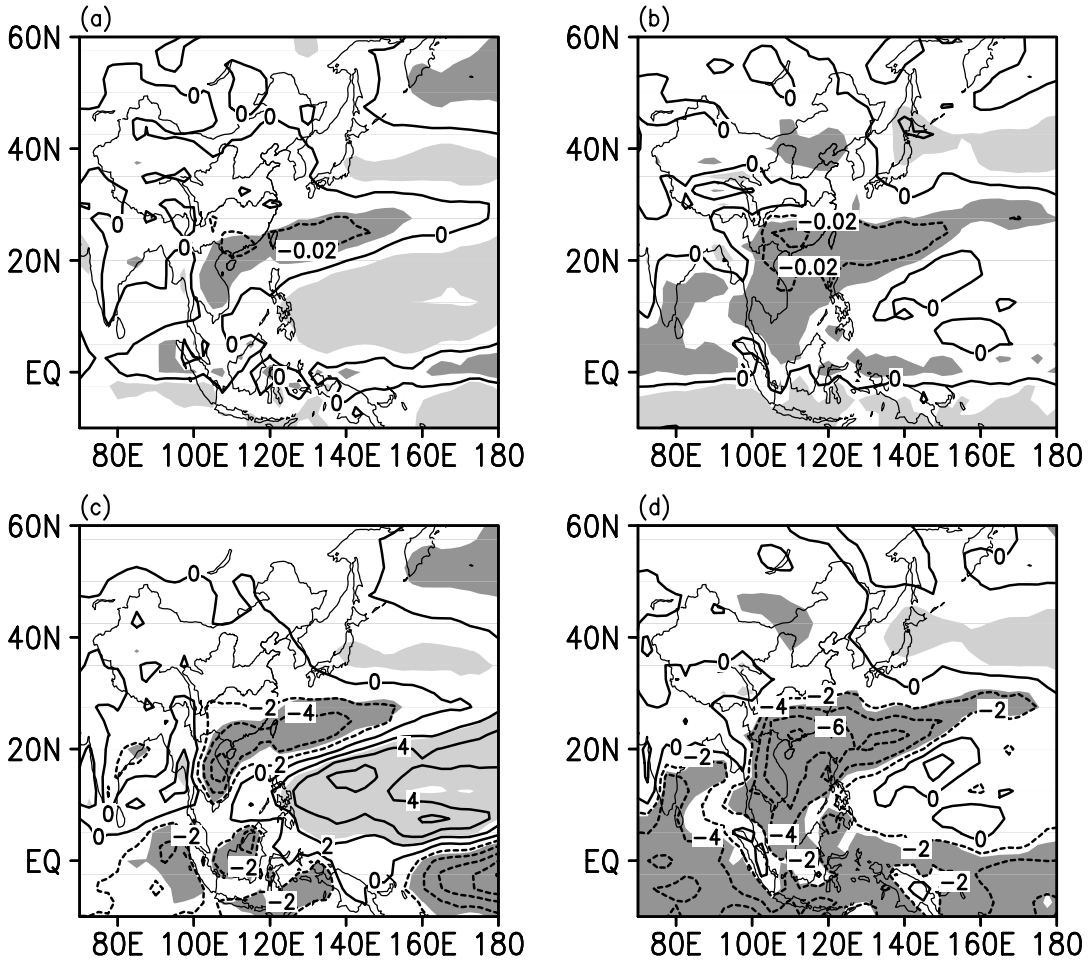

Fig. 11. Regression of JFM 700-hPa potential vorticity (units: 10^6 K m^2 Kg^{-1} s^{-1}) (a) and convective instability (c) (units: 10^5 K Pa^{-1}) with respect to normalized DJF Niño-3 SST. (b) and (d) are the same as (a) and (c) except for DJF SCS SST. Shading denotes regions with correlation significant at 0.05 level.